Available online at www.sciencedirect.com

ScienceDirect

Proceedings of the Combustion Institute 35 (2015) 1701–1708

Proceedings of the Combustion Institute

www.elsevier.com/locate/proci

Multistage oscillatory "*Cool Flame*" behavior for isolated alkane droplet combustion in elevated pressure microgravity condition

T.I. Farouk [a,*], M.C. Hicks [b], F.L. Dryer [c]

[a] *Department of Mechanical Engineering, University of South Carolina, Columbia, SC 29208, USA*
[b] *NASA Glenn Research Center, Cleveland, OH 44135, USA*
[c] *Department of Mechanical and Aerospace Engineering, Princeton University, Princeton, NJ 08544, USA*

Available online 16 July 2014

Abstract

Recently, large diameter, isolated *n*-heptane droplet experiments under microgravity conditions (aboard the International Space Station) exhibited "*Cool Flame*" burning behavior, resulting from a heat loss mechanism that extinguishes hot combustion and a transition into a sustained, low temperature second stage combustion. In atmospheric pressure air, a single combustion mode transition to "*Cool Flame*" burning is followed by diffusive extinction. But with increasing pressure, *multiple cycles* of hot initiation followed by transition to "*Cool Flame*" burning are observed. This paper reports experimental observations that characterize the transition time histories of this multi-cycle, multi-stage behavior. Transient spherosymmetric droplet combustion modeling that considers multi-stage detailed kinetics, multi-component diffusion, and spectral radiation is applied to analyze the experimental observations. The simulations indicate that as parameters change the chemical time scales dictating low temperature degenerate chain branching, multiple hot/cool flame burning transitions are induced by increasing the cool flame burning heat generation rate compared to the diffusive loss rate. The balance of these terms in the negative temperature coefficient kinetic regime defines whether reactions accelerate into re-ignition of a hot flame event, burn quasi-steadily in the cool flame mode, or diffusively extinguish. The rate of reactions controlling ketohydroperoxide formation and destruction are shown to be key re-ignition of hot combustion from the cool flame mode. Predictions are found to be in good agreement with the experimental measurements. Modeling is further applied to determine how these observations are dependent on initial experimental conditions, including pressure, and diluent species.

Keywords: Cool Flame; Droplet combustion; Microgravity; Radiation; FLEX

1. Introduction

Since their discovery, "*Cool Flames*" have intrigued researchers over the years. Classically, the term "*Cool Flame*" is associated with premixed systems in which a transient

* Corresponding author. Fax: +1 803 777 0106.
E-mail address: tfarouk@sc.edu (T.I. Farouk).

http://dx.doi.org/10.1016/j.proci.2014.06.015
1540-7489/

propagating wave proceeds through a premixed fuel/air mixture with one or more repetitive occurrences leading to high temperature burning of the remaining reactants. Quasi-steady, cool flame phenomena have also been produced in flowing premixed reactants, typically followed by a second stage hot flame. Bradley and coworkers [1] studied cool flame and second-stage ignition phenomena in a quasi-steady configuration by using a vertical flow reactor arrangement and the oxidations of acetaldehyde or propionaldehyde. Fairlie et al. [2,3] studied transient "*Cool Flames*" and the associated repetitive phenomena using premixed propane–oxygen static reactor experiments in microgravity. Their study involved both experimental and numerical aspects. The onset, spatial growth and stability of the "*Cool Flame*" was attributed to the interactions among the elementary reactions and rates governing negative temperature coefficient (NTC) behavior and the temperature field controlled by thermal diffusion to the reactor wall. In their pioneering work, Tanabe et al. [4] reported the two-stage ignition behavior of *n*-heptane droplets. Time dependent temperature field around the igniting droplets were observed by interferometry to determine the two step temperature rise. Moriue et al. [5] utilized the tethered droplet configuration to experimentally measure the ignition delays of "*Cool Flame*" and hot flame appearance for single *n*-decane, *n*-dodecane, *n*-tetradecane and *n*-hexadecane droplets in a multiphase system. The flames were produced by inserting the droplet in a temperature controlled furnace and observing flame evolution using Michelson interferometry. Cuoci et al. [6] simulated Moriue's *n*-decane experiments with a detailed hydrocarbon oxidation mechanism. Their model was able to predict the multi-stage ignition behavior.

Recently, long duration, "*Cool Flame*" burning for large diameter, isolated droplet combustion was first observed for atmospheric pressure, pure *n*-heptane droplets experiments in air aboard the International Space Station (ISS) [7,8]. In these non premixed experiments, large *n*-heptane droplet burning exhibited dual modes of combustion and extinction. In the first stage following ignition, the droplet underwent classical high temperature burning with a visible flame surrounding the droplet. The transient, high temperature burning was observed to extinguish radiatively, followed by a continuing lengthy period of quasi-steady surface regression of the droplet without any visible flame. This lengthy "*second stage*" phenomenon was observed to extinguish, leaving behind a smaller droplet, which experienced a short period of time-dependent evaporation.

Detailed numerical analysis of these experiments [8] indicates that the "*second stage*" behavior results from the existence of multistage kinetic regimes that are well known in terms of two stage autoignition phenomena [9–11] and the premixed "*Cool Flame*" phenomena with large carbon number normal alkanes [12]. In the "second stage", heat generation as a result of negative temperature coefficient, degeneratively branched, oxidation chemistry was shown to be dynamically balanced by diffusive heat loss, leading to the lengthy period of "flameless" quasi-steady droplet regression, concluded by diffusive extinction. Though the phenomena are different in principle from those governing classical premixed cool flames, the low temperature droplet burning behavior has been generally conotated as "*cool flame*": droplet burning. It is not surprising that similar observations would occur with even larger carbon number normal alkanes such as *n*-octane, *n*-decane, etc., all of which have more rapid negative temperature coefficient kinetic rates than *n*-heptane [13]. More recent ISS *n*-heptane isolated droplet combustion experiments at three atmospheres pressure and the same oxygen index but with diluents inhibiting heat loss shows "multiple cycles" of dual stage combustion i.e. *hot–cool* flame transitions. This paper presents experimental examples of this multistage, multiple cycle mode of isolated *n*-heptane droplets under high pressure microgravity conditions. The experimental observations are then compared against *apriori* detailed numerical predictions using a novel spherosymmetric droplet combustion model that includes full multi-stage detailed chemical kinetics, multi-component transport, and spectral radiative interactions. Predictions from the model are found to compare favorably with the experimentally measured droplet and flame diameter evolution histories, and diffusive extinction results. Further modeling calculations are analyzed to elucidate the effects of different ambient conditions; i.e. pressure and diluent concentration.

2. Experimental setup and procedure

The experiments are conducted under the **FL**ame **EX**tinguishment (FLEX) program onboard the International Space Station (ISS). The Multi-User Droplet Combustion Apparatus (MDCA) installed in the Combustion Integrated Rack (CIR) facility was employed. The MDCA uses an opposed needle deployment technique [14] to deploy droplets of chosen diameter on an 80 μm single filament silicon carbide (SiC) fiber in these microgravity experiments (freely floating droplet experiments can also be performed). The tethering fiber was necessary for these tests in elevated pressure in order to eliminate the relative velocity between the gas phase and the droplet upon deployment. Ignition of the tethered droplet was accomplished using two symmetrically positioned Kanthal hot wire igniters. The experimental diagnostic system consisted of a black-white cam-

era to capture back-lit droplet images to obtain the droplet diameter regression. The illumination for the backlit view is a red laser diode source and a collimating optical system which provide monochromatic illumination with a center wavelength between 650–660 nm. The laser diode operates below the lasing threshold current and acts as a non-coherent illumination source. A UV sensitive flame-imaging camera is used to observe OH^* - chemiluminescence at 310 nm wavelength to measure the flame diameter evolution, and a color CCD camera with a wider view angle to monitor the experiments. All the camera images were captured at 30 fps. The entire CIR is mounted to the ISS through the Passive Rack Isolation System (PaRIS) and the quality of microgravity during testing is verified by measurements made from the Space Acceleration Measurement System (SAMS). The PaRIS serves to isolate the experiments from high frequency vibration or *g*-jitter by allowing full disengagement of the CIR from the ISS structure. Measurements from the SAMS indicated that gravity levels less than 10^{-5} of Earth's normal gravity are maintained during the experiments. Further details of the experimental setup can be found in Dietrich et al. [15].

Experiments are typically conducted for larger droplet sizes, $d_o \sim 3$–5 mm, with *n*-heptane as the fuel. For every experiment the combustion chamber is filled with the desired ambient gas mixture, consisting of oxygen, nitrogen and carbon dioxide to a pressure of 3.0 atm. The droplet diameters are obtained using a frame-by-frame analysis of individual digital images captured by the black–white camera using ImageJ [16]. Flame diameters are obtained similarly from the images captured by both the UV and color CCD camera.

3. Numerical modeling

The high pressure *n*-heptane droplet combustion experiments were numerically simulated employing a novel and comprehensive multiphase droplet combustion model. The transient spherosymmetric droplet combustion model considers multistage detailed gas phase kinetics, spectrally resolved radiative heat transfer, and multi-component transport in solving the species and energy conservation equations for both the liquid and gas phase. Coupling of the liquid and gas interface satisfies thermodynamic constraints and conservation of material fluxes. Gas phase radiant interactions are incorporated using a statistical narrow band (SNB) radiation submodel [17] a critical issue in modeling radiation with participating medium (e.g. carbon-dioxide which acts both as a emitter and absorber) as well the pressure dependence of absorption. The model also includes the heat transfer perturbations due to the presence of the tether fiber that considers conduction, convection as well as radiative losses. The heat transfer effect through the tether fiber is included using a transient, one dimensional model. Due to the small size of the fibers employed ($d_{fiber} = 80$ μm) and the associated small Biot numbers, the temperature distribution in the tether fiber can be assumed to be one dimensional. The ignition source was simulated by providing an initial trapezoidal temperature profile having a peak temperature of 2200 K. Details of the model are further described in publications [18–21].

In the simulations, the liquid phase properties are calculated from the data correlations of Daubert and Danner [22]. Temperature dependent thermo-physical and transport properties of the SiC tether fiber [23] were also employed. In order to resolve the effects of the low and high temperature kinetics a detailed *n*-heptane chemical kinetics model [24] is employed, in a mathematically reduced form described in detail in [8].

4. Results and discussion

Five successful experiments were conducted for CO_2 diluent exchange tests at 3 atm (FLEX 476, 477, 480, 485 and 486). In all these experiments, the oxygen concentration was held constant at 21% and CO_2 was systematically varied in a N_2 balance environment. All these experiments showed multiple high-low temperature combustion stages. In this paper, we only present and analyze the FLEX 480 experimental data. The experimental conditions are $d_o = 4.08$ mm, 0.21 X_{O2}, 0.15 X_{CO2}/balance N_2, at three atmosphere pressure and is referred to as the base case. Droplet burning rates are calculated for each combustion regime; i.e., the high temperature burning regime and the low temperature second stage burning regime. The burning rates for the second stage ignition phase are calculated for the period of time between the extinction of the visible flame and the subsequent re-ignition event. In three of the tests the second stage burning regime is further segmented by an additional re-ignition event and, as such, a second burning rate is calculated for the period of time between the first and the second re-ignition events. The time, at which the visible flame extinguishes and at which the subsequent re-ignition events occur have been recorded. All times are referenced to $t = 0$ s at the time the igniters are retracted. For the FLEX 480 experiment, the burning rates and occurrence times for the different combustion stages are as follows: Visible flame (high temperature) burning rate = 0.86 mm^2/s, Visible flame extinction at $t_b = 8.3$ s, First low temperature burning rate = 0.79 mm^2/s, First re-ignition at $t_b = 12.7$ s, Second low temperature burning rate = 0.66 mm^2/s, Second re-ignition at $t_b = 18.2$ s.

In each test the flame steadily grows in diameter and decreases in luminous intensity to the point at which it reaches its maximum diameter where it then either suddenly extinguishes or begins to exhibit oscillatory behavior just prior to extinguishing. The oscillatory behavior is marked by repeated transitions between a complete and partial spherical flame surface and lasts for a brief period of time before completely extinguishing. The extinction of the visible flame commences the low temperature second stage burning regime, qualitatively referred to as the "*Cool Flame*" regime. During the second stage burning, rapid droplet vaporization persists and is only momentarily interrupted by the occurrence of one or more hot flame re-ignition events, typically lasting less than 1.0 s. The re-ignition event is initiated from a small region on the spherical surface that is eventually defined by a fully enveloping, re-ignited hot flame. This re-ignited high temperature flame has a diameter significantly larger than the preceding high temperature flame which had previously radiatively extinguished. An example of this re-ignition is shown in Fig. 1 where a sequence of images taken sequentially every 0.033 s shows the re-ignition kernel and the resulting flame wrapping around the contour of a spherical shell, presumably defining the stoichiometric surface. The re-ignited high temperature flame is not sustainable because, as with the original flame, its hypothetical flame radius without radiative loss exceeds that radius at which radiation loss exceeds heat generation.

Figure 2 shows the predicted droplet diameter and flame diameter evolution along with the experimental measurements of FLEX 480. It can be seen that the predictions from the model agree favorably with the experimental measurement and captures all of the qualitative trends of the intricate features; especially the multi-cycle two stage burning. The predicted droplet diameter regression rate is slower in comparison to the experiment. Likely experimental sources that may perturb the spherosymmetric result include slow gas/drop convection as a result of residual droplet drift [25] and movement along the tethering fiber, both of which may affect burning rate and the incomplete spherical flame structure/oscillatory behavior noted during transitions from low temperature burning to the second hot burning phase. It is apparent that in comparison to the FLEX experiments at atmospheric pressure [8,15] the measured droplet diameter regression rates at elevated pressures show significantly greater departures from the local time averaged values. There exist multiple non-linear regimes in the droplet

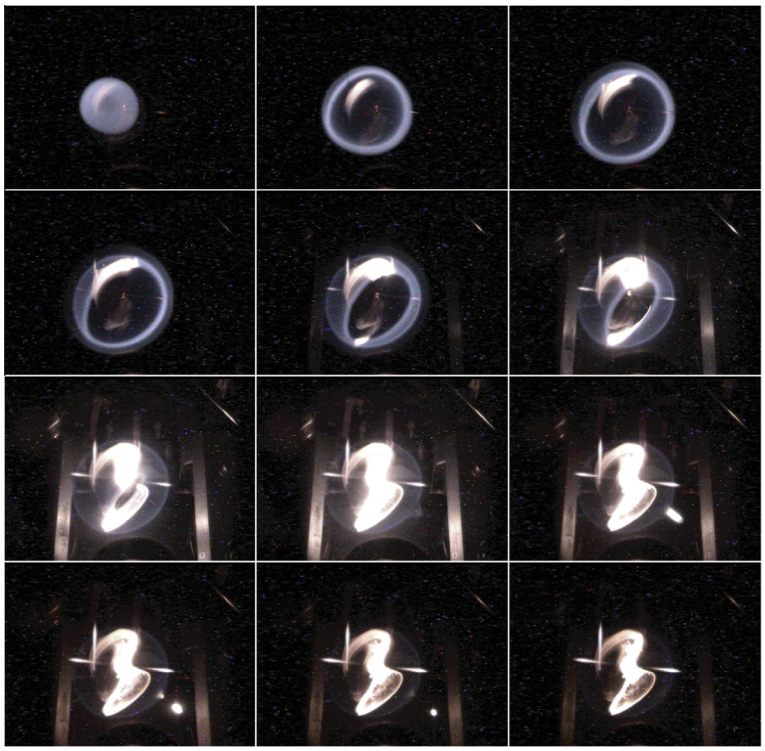

Fig. 1. Image montage from FLEX Test 480 showing the progression of the final hot flame re-ignition starting at $t = 18.4$ s with each image spaced 0.033 s apart ($d_o = 4.08$ mm, 0.21 X_{O2}, 0.15 X_{CO2}/balance N_2, 3 atm).

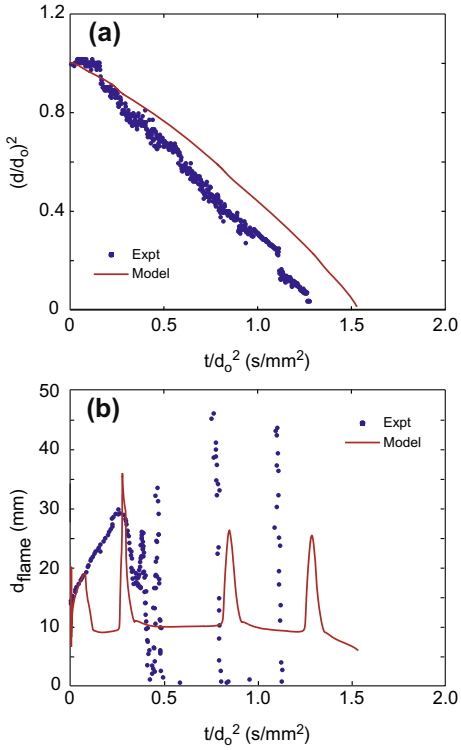

Fig. 2. Measured and predicted evolution of: (a) droplet diameter and (b) flame diameter for a *n*-heptane droplet combustion. Simulation conditions are identical to FLEX Test 480.

diameter regression rates which are not apparent in the locally time averaged burning history, but are clearly distinguishable in the instantaneous burning rate evolution (Fig. 3). The flame diameter evolution presented in Fig. 2b shows an example of this dynamic behavior. Initially the flame diameter is found to be large and together with

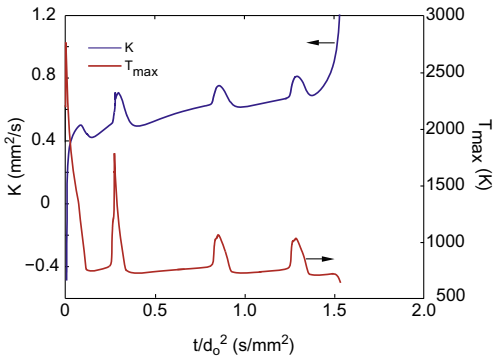

Fig. 3. Predicted temporal evolution of burning rate and peak gas temperature for a *n*-heptane droplet combustion under conditions identical to FLEX Test 480.

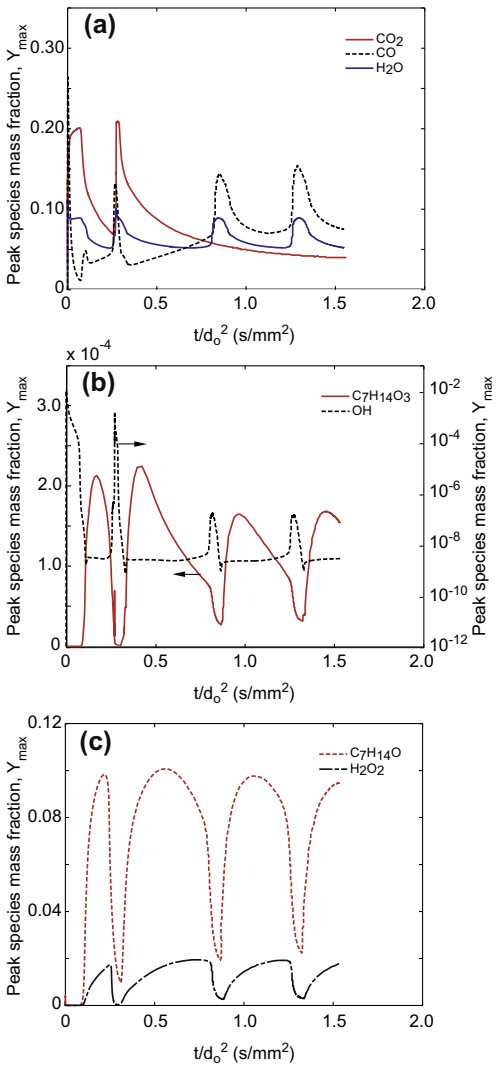

Fig. 4. Temporal evolution of peak temperature and species mass fraction: (a) temperature, CO_2, H_2O and CO (background ambient concentration subtracted for CO_2), (b) ketohydroperoxide ($C_7H_{14}O_3$) and OH and (c) cyclic ethers ($C_7H_{14}O$) and H_2O_2. The ketohydroperoxide and cyclic ether are the total peak concentration of the different species. Simulation conditions are identical to that of FLEX Test 480.

the peak temperature evolution presented in Fig. 3 it is indicative of high temperature burning. Following the initial high temperature burn, the flame diameter is observed to decrease rapidly as a result of radiative heat loss (Fig. 5), and transitions to the first low temperature/"*Cool Flame*" mode. Three subsequent initiations of transient hot flame burning of very short duration are each followed by a longer duration, "*Cool Flame*" burning period. In every *hot-cool flame* transition, the flame diameter is found to decrease by

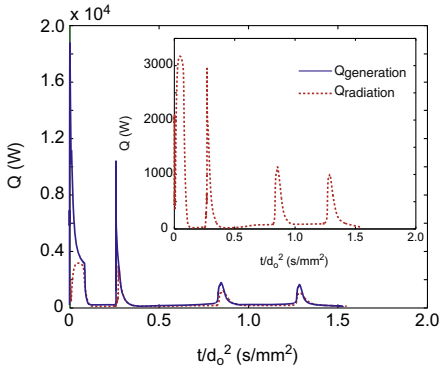

Fig. 5. Total heat generation and radiative heat loss for a *n*-heptane droplet undergoing multi-cycle two-stage combustion. Inset showing radiative heat loss only. Simulation conditions are identical to that of FLEX Test 480.

~40–50% of the prior cycle, maximum hot flame radius. Based on the predicted flame diameter evolution, the first transition to "*Cool Flame*" (i.e. visible flame extinction) is observed at $t_b = 2.4$ s, the first re-ignition at $t_b = 4.64$ s, the second and the third/last re-ignition occurring at $t_b = 14.56$ s and $t_b = 21.64$ s. The predicted onset of second and third re-ignition that coincides with the experimentally observed 'first' and 'second' cases differs by ~2 s. However, the difference between the predictions and measurements during the very early stages ($0 \leqslant t_b \leqslant 5.0$ s) are likely the result of non-idealities in experiment and modeling of the experimentally aspherical, but symmetric hot wire ignition energy addition method. The initial ignition energy is known to significantly affect the transient establishment of the initial high temperature burning phase [26].

The predicted evolution of the instantaneous burning rate and peak gas temperature for the base case are presented in Fig. 3. The predicted K evolution shows a large negative value at the initial state of the burn occurring as the droplet diameter increases due to the thermal expansion. A sharp rise in K occurs towards the end of the burn as the droplet diameter becomes comparable to the fiber diameter with additional heat flux from the fibers becoming significant. The multi-cycle oscillatory burning is apparent; with K being lower during the "*Cool Flame*" mode. It is evident that the as the droplet progresses through the burn, multiple transitions between *hot–cool* flame burning rates are observed. Closer scrutiny of the peak gas temperature evolution reveals that only one hot re-ignition takes place during the combustion processes. Apparently, the second and third pulses do not result in a hot flame as can be seen by the peak value of the temperature for each pulse. The peak gas temperatures in the second and third pulse are ~1070 K which is considerably lower than that needed to achieve high temperature chemically branched reaction, as further evidenced by the CO_2 temporal profile (Fig. 4a). Thus, the second and third pulses are unsteady transitions phenomena entirely resident with the intermediate temperature kinetic regime.

Temporal evolution of the peak concentrations of some of the dominant species are depicted in Fig. 4. It can be seen that the temporal evolution of the peak species concentration sharply delineates the two distinct combustion stages – high temperature and low temperature burning. During high temperature burning, the major products of combustion are CO_2 and H_2O (Fig. 4a). But as a transition to low temperature burning occurs, the rate of production of CO_2 decreases drastically, while its precursor species, i.e. CO, accumulates. Additionally, the temporal evolution of peak CO_2 shows that after the first hot-cool flame transition, only one hot flame re-ignition occurs at $t_b = 4.64$ s. Beyond $t_b = 4.64$ s, the peak CO_2 concentration steadily decreases. No further sharp rises in CO_2 concentration indicating CO oxidation are observed for the second and third pulses observed in K and T_{max}.

Second stage temperatures are too low to achieve hot flame chemically chain branched burning and do not support oxidation of the CO on available reaction timescales in the burning region. Interestingly the second and third pulses in K and T_{max} coincide with the latter increases of CO. The low and high temperature reactive character is also characterized by increasing ketohydroperoxide and OH (Fig. 4b), with high concentration of ketohydroperoxide denoting low temperature combustion. The peak cyclic ether ($C_7H_{14}O$) and H_2O_2 temporal evolution are shown in Fig. 4c. The increase and decrease in H_2O_2 coincides with the $C_7H_{14}O$ evolution. Characteristic of NTC kinetic behavior, the $C_7H_{14}O$ are formed by the decomposition of $C_7H_{14}OOH$ resulting in a chain propagation of OH. Hydrogen peroxide is produced from $C_7H_{14}O$ when reacting with OH or HO_2. The degenerate branching condition associated with ketohydroperoxides increases the reactivity of the system with limited heat release. As temperature increases, peroxy radical decomposition is favored, reducing the overall reactivity. The unsteady nature of the system results from crossing of the NTC into the hot ignition condition, followed by a return to cool flame burning in the NTC regime. The observed phenomenon is associated with a dynamics resulting from imbalance in heat generation/heat loss associated with crossing the hot ignition condition (Fig. 5). Sufficient heating occurs in comparison to heat losses during the re-established cool flame burning to drive the system again into a hot "reignition" condition. However, during each subsequent re-ignition, the stoichiometric fuel/oxygen location is moving substantially to a larger radial

location (towards the far field) as more partially oxidized fuel vapor accumulates surrounding the droplet. During each subsequent re-ignition event, the governing result is a reduction in heat generation in comparison in prior case. CO builds up as subsequent cool flame burning and re-ignition events occur, with essentially no conversion to carbon dioxide.

In order to assess the influence of pressure on multi-cycle burning behavior, simulations were conducted over a range of pressure. The effect of pressure on the burning rate and the flame diameter is summarized in Fig. 6. For pressures lower than 3 atm only a single two stage combustion event is observed, followed by extinction of the "*Cool Flame*" burning period. As the pressure increases the multi-cycle behavior emerges, with the transition from a single to two cycle behavior at a pressure between 3 and 3.5 atm. With increasing pressure, the "turnover temperature", i.e. the temperature at which NTC behavior first initiates, and the hot ignition temperature both increase (Fig. 6a inset). At higher pressures the heat generation during the "*Cool Flame*" heat generation increases at a faster rate compared to the diffusive heat loss causing the "*Cool Flame*" temperature to slide toward a higher temperature and eventually cross into hot ignition (Fig. 6b inset). To further elucidate the role of heat losses on the "*Cool Flame*" behavior, [8], simulations at elevated pressures were conducted with varying ambient diluent concentrations of CO_2, a radiatively participating diluent but which has a lower thermal diffusivity in comparison to nitrogen (Fig. 7). By introducing a small amount of CO_2 prompts the multi-cycle behavior. The presence of CO_2 in the ambient enhances the radiative heat loss during the high temperature burn but reduces the diffusive heat loss during the low temperature "*Cool Flame*" burning mode. As a result the heat generation during the low temperature burn drives the system into hot ignition. It is also observed that by increasing the CO_2 concentration the transitions to *hot-cool* flame cycles occur earlier.

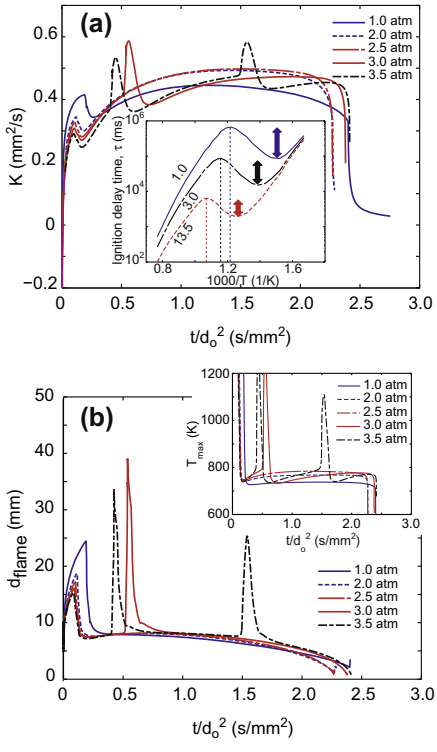

Fig. 6. Predicted temporal evolution of burning rate and flame radius for a untethered *n*-heptane droplet combustion in different operating pressure. ($d_o = 3.5$ mm, 0.21 X_{O2}, 0.15 X_{CO2}/balance N_2). Inset of ignition delay time as a function of temperature for different operating pressure and zoomed inset of T_{max} evolution during the low temperature burn is also presented.

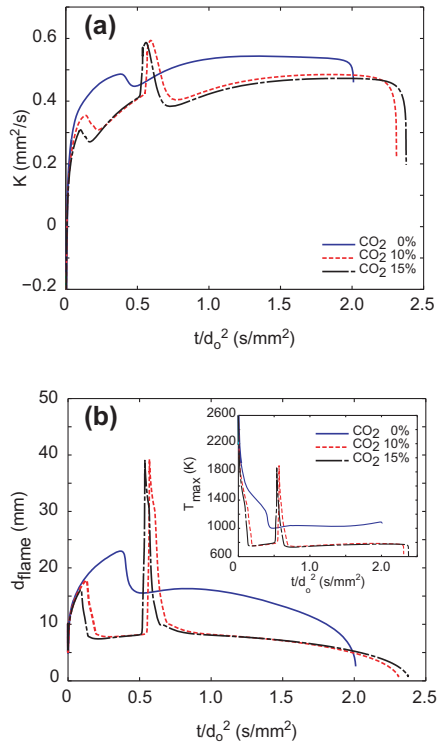

Fig. 7. Predicted temporal evolution of burning rate and flame radius for a *n*-heptane droplet combustion in varying ambient CO_2 concentration ($d_o = 3.5$ mm, 0.21 X_{O2}. varying X_{CO2}/balance N_2, 3 atm). Inset showing the peak temperature evolution is also presented.

5. Summary

Experimental data of large diameter *n*-heptane droplet combustion at elevated pressure is reported. A unique multi-cycle *hot-cool* flame burning is observed where a droplet starting as hot flame transitions to a "*Cool Flame*" and then reignites to a hot flame followed by unsteady *Cool Flame*'*s* depending on the initial droplet diameter. Simulations of these experiments are conducted using a transient spherosymmetric model with detailed chemistry that included both high temperature and low temperature kinetics. *Apriori* predictions were found to be in qualitative (even semi quantitative) agreement with all the experimental observations. Quantitative differences likely arise from both the inaccuracies in the modeling assumptions and submodels, as well as experimental aberrations from the ignition event and other asymmetric behaviors. Simulations indicate that the multi-cycle, two stage burning behavior observed in the present experiments and prediction by the modeling results is controlled by the relative rates of heat generation and diffusive loss in the "*Cool Flame*" burning mode. Variations in the droplet combustion environmental parameters (diluent, oxygen index, pressure), drop size, and kinetics (through fuel properties) should all result in changes in heat generation/heat loss that lead to the absence of two stage burning behavior [6], and the multi-cycle behaviors discussed in this work.

Acknowledgements

The financial support of the USC startup fund (for TIF) and National Aeronautics and Space Administration through Grant Number NNX09AW 19A (for FLD) is acknowledged.

References

[1] J.N. Bradley, G.A. Jones, G. Skirrow, C.F.H. Tipper, Tenth Symposium (International) of Combustion, 139–144, 1965.
[2] R. Fairlie, J.F. Griffiths, H. Pearlman, *Proc. Combust. Inst.* 28 (2000) 1693–1699.
[3] R. Fairlie, J.F. Griffiths, K.J. Hughes, H. Pearlman, *Proc. Combust. Inst.* 30 (2005) 1057–1064.
[4] M. Tanabe, M. Kono, J. Sato, J. Koenig, C. Eigenbrod, F. Dinkelacker, H. RathZarm, *Combust. Sci. Technol.* 108 (1995) 103–119.
[5] O. Moriue, C. Eigenbrod, H.J. Rath, M. Tsue, M. Kono, J. Sato, *Trans. Jpn. Soc. Aerospace Sci.* 47 (157) (2004) 189–194.
[6] A. Cuoci, M. Mehl, G. Buzzi-Ferraris, T. Faravelli, D. Manca, E. Ranzi, *Combust. Flame* 143 (2005) 211–226.
[7] V. Nayagam, D.L. Dietrich, P. Ferkul, M.C. Hicks, F.A. Williams, *Combust. Flame* 159 (2012) 3583–3588.
[8] T. Farouk, F. Dryer, *Combust. Flame* 161 (2014) 565–581.
[9] S. Jahangirian, S. Dooley, F.M. Haas, F. Dryer, *Combust. Flame* 159 (1) (2012) 30–43.
[10] H.J. Curran, P. Gaffuri, W.J. Pitz, C.K. Westbrook, *Combust. Flame* 114 (1998) 149–177.
[11] C.K. Westbrook, W.J. Pitz, O. Herbinet, H.J. Curran, E.J. Silke, *Combust. Flame* 156 (1) (2009) 181–199.
[12] V. Nayagam, D. Dietrich, M.C. Hicks, F. Williams, in: 29th Annual Meeting of the American Society of Gravitational and Space Research, Orlando, Florida, 2013.
[13] P.S. Veloo, S. Jahangirian, F.L. Dryer, in: *Spring Technical Meeting of the Central States Section of the Combustion Institute*, Dayton, Ohio, 2012.
[14] V. Nayagam, J.B. Haggard Jr., R.O. Colantonio, A.J. Marchese, F.L. Dryer, B.L. Zhang, F.A. Williams, *AIAA J.* 36 (8) (1998) 1369–1378.
[15] D. Dietrich, Technical Publication NASA/TP-2013-216046 (2013) NASA, Glenn Research Center, Cleveland OH 44135, USA, December 2013.
[16] M.D. Abramoff, P.J. Magelhaus, S.J. Ram, *Biophotonics Intl.* 11 (7) (2004) 36–42.
[17] Z. Chen, X. Qin, B. Xu, Y. Ju, F. Liu, *Proc. Combust. Inst.* 31 (2) (2007) 2693–2700.
[18] T. Farouk, F.L. Dryer, *Combust. Flame* 159 (2012) 200–209.
[19] A.J. Marchese, F.L. Dryer, V. Nayagam, *Combust. Flame* 116 (1999) 432–459.
[20] T.I. Farouk, F.L. Dryer, *Combust. Flame* 159 (2012) 3208–3233.
[21] T. Farouk, F.L. Dryer, *Combust. Theor. Model.* 15 (4) (2011) 487–515.
[22] T.E. Daubert, R.P. Danner, *Physical and Thermodynamic Properties of Pure Chemicals: Data Compilation*, Hemisphere Publishing, New York, 1989.
[23] E. Youngblood, D.J. Senor, W. Kowbel, J. Webb, A. Kohyama, Thermophysical and mechanical properties of SiC/SiC composites, US DOE, Office of Fusion Energy Sciences, 1999.
[24] H.J. Curran, P. Gaffuri, W.J. Pitz, C.K. Westbrook, *Combust. Flame* 129 (2002) 253–280.
[25] M.Y. Choi, F.L. Dryer, J. Haggard, *Proc. Combust. Inst.* 23 (1990) 1597–1604.
[26] T. Farouk, Y.C. Liu, A.J. Savas, C.T. Avedisian, F.L. Dryer, *Proc. Combust. Inst.* 34 (1) (2013) 1609–1616.